LIGO-T970238-00-D
HYTEC-TN-LIGO-13
01/15/97

HAM Seismic Isolation
Projected Performance Update

Eric Ponslet
January 15, 1997

Abstract

This notes summarizes performance predictions of the current designs for the HAM seismic isolation systems. Three configurations using the baseline Viton rubber spring and two damped metal spring designs (multi-layer coil spring and leaf spring) are considered. Vertical and horizontal transmissibilities are evaluated as well as residual mirror motions due to floor seismic noise in the horizontal and vertical directions.

HYTEC Inc.
110 Eastgate Dr., Ste 100
Los Alamos, NM 87544
(505) 662-0080 / Fax (505) 662-5179

LIGO PROJECT

1. HAM Seismic Isolation - System Description

The current design layout for the HAM SEI is shown in Fig. 1. The global coordinate system used throughout this document is shown in the figure. Its origin is on the facility floor along the vertical axis of the optics table, the *Z* axis is pointing vertically up and the *X* axis is parallel to the internal support beams. Rotations *a* (roll), *b* (pitch), and *c* (yaw) are also defined.

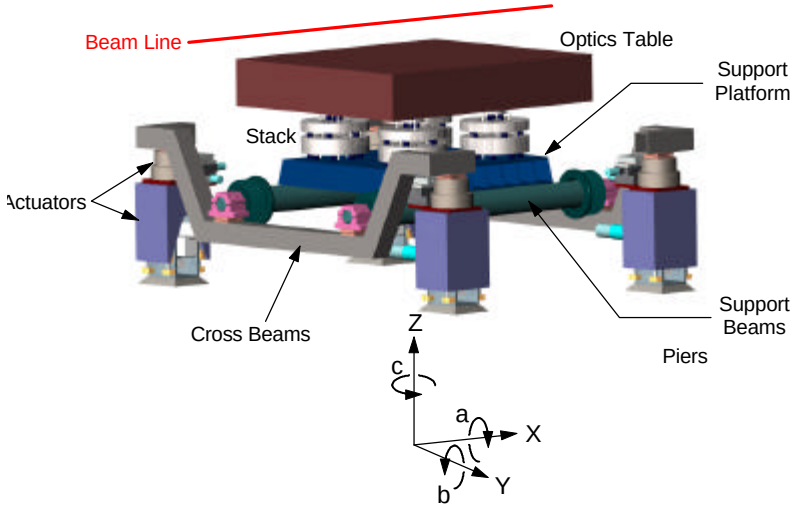

Figure 1: overall configuration of HAM seismic isolation system.

We distinguish two separate subsystems: the support structure and the isolation stack. The support structure consists of the coarse actuation system, external cross beams, internal support beams, and support platform. It is described in reference 1. The stack[2] consists of 4 legs of springs and stainless steel masses, the optics table[3], and the payload (optics, etc.). Note that , because isolation requirements are much looser on the HAM stacks, all HAM stacks have been designed with 3 stages instead of the 4 stages used in the BSC stacks.

The stack provides seismic isolation for the optics table and is responsible for the largest part of this isolation at low frequencies. However, the support structure is not infinitely rigid and contributes to isolation at higher frequencies (above 50 Hz or so) while its resonances degrade isolation at lower frequencies[1]. The major sources of compliance in the support system are the actuators (horizontal compliance) and the cross beams and support tubes (vertical compliance)[1]. However, because the HAM isolation performance is much better than required at all frequencies, there is little risk of requirement violations caused by support assembly resonances at any frequency, as long as the Q of those resonances can be kept below a few hundreds. For that reason, modeling support dynamics is not essential and all predictions presented in this document were generated from models of the stacks only.

2. Design Requirements

The main design requirement is a limit on the horizontal transmissibility of the SEI system (Fig. 2 and [4]). There is no explicit requirement on vertical transmissibility.

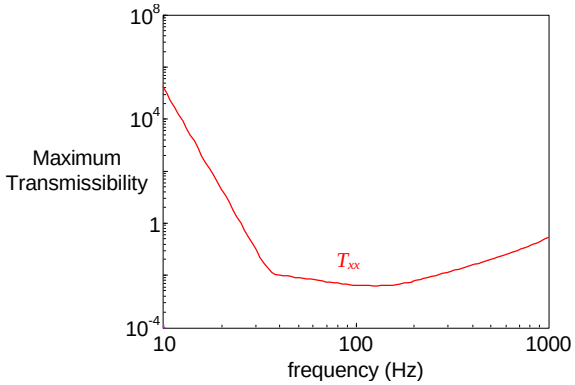

Figure 2: Approximate transmissibility requirement for HAM SEI[4].

3. Modeling

3.1 Assumptions

All stack elements and the optics table are modeled as rigid bodies[5] (their natural frequencies are above 250 Hz). Spring resonances are neglected (springs are designed so that first resonant frequency is above 400 Hz[6]).

The attachment point of the mode-cleaner mirrors suspension wires is assumed to be at X = 0 cm, Y = 0 cm, and Z = 42.6 cm with respect to the center of the top surface of the optics table. The transmissibilities of the SEI system are evaluated from the facility floor to that point.

3.2 Support Structure Dynamics

Because the isolation performance of the HAM stacks is much better than required at all frequencies, the support assembly dynamics was not included in the models. Clearly, support assembly resonances will create peaks in the response curves that will degrade isolation performance in narrow frequency ranges. However, as long as the Q of those resonances can be expected to be of the order of a few hundreds of less, the horizontal isolation requirement will not be violated.

3.3 Evaluation of Residual Mirror Motion

The mode-cleaner mirror penduli are attached to the optics table of the SIS. Assuming that the moving masses in those mirror suspension systems are small in magnitude compared to the optics table, we can treat the complete assembly as 2 linear systems connected in series. Calculation of the spectrum of X motion of the mirror's suspension point simply requires combining the effects of the direct horizontal transmission and the vertical to horizontal coupling terms.

The following assumptions are made:

- the only important contributions from the floor seismic noise are the *X* and *Z* motions. The *X* and *Z* noise spectra are assumed identical[4].
- the SUS transfer functions produce horizontal mirror motion from optics plate motion in the horizontal (T_{xx}^{SUS}), vertical (T_{xz}^{SUS}), yaw (T_{xc}^{SUS}), and pitch (T_{xb}^{SUS}) directions. The magnitudes of these transfer functions[6,10] are plotted in Fig. 3; they are assumed identical to those of the test mass suspension system. Note that T_{xx}^{SUS} is at least 1 order of magnitude larger than the other transfer functions.
- the horizontal and vertical motions of the floor are assumed uncorrelated.

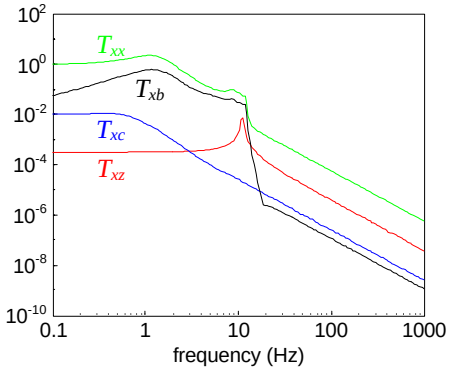

Figure 3: transmissibilities of the SUS system (X motion of test mass in response to optics table motion in X, Z, b (pitch), and c (yaw) directions[6,10]).

With these assumptions, the PSD of the residual mirror motion in the horizontal direction X_{mirror}^2 is evaluated from the PSDs of floor motion in the horizontal and vertical directions (X_{floor}^2 and Z_{floor}^2) as

$$X_{mirror}^2 = \left[T^{SEI+SUS}\right] \cdot \begin{bmatrix} X_{floor}^2 & 0 \\ 0 & Z_{floor}^2 \end{bmatrix} \cdot \left[T^{SEI+SUS}\right]^*, \qquad (1)$$

where * denotes the adjoint operator and $\left[T^{SEI+SUS}\right]$ is a matrix of transfer functions for the complete isolation and suspension system and is evaluated as

$$\left[T^{SEI+SUS}\right] = \left[T_{xx}^{SUS} \quad T_{xz}^{SUS} \quad T_{xb}^{SUS} \quad T_{xc}^{SUS}\right] \cdot \begin{bmatrix} T_{xx}^{SEI} & T_{xz}^{SEI} \\ T_{zx}^{SEI} & T_{zz}^{SEI} \\ T_{bx}^{SEI} & T_{bz}^{SEI} \\ T_{cx}^{SEI} & T_{cz}^{SEI} \end{bmatrix}, \qquad (2)$$

where all *T* 's are complex functions of frequency. The complete 4×2 matrix of SEI transfer functions is evaluated with our 3D Matlab code.

3.4 Calculation of Figures of Merit for Lock Acquisition

The lock acquisition figure of merit is the RMS velocity of the mirror in response to residual seismic noise, with the mirror pendulum damped by the SUS control system. This

RMS velocity is in principle derived directly from the mirror motion PSD, X^2_{mirror} as follows:

$$V_{RMS} = \sqrt{\int_{f=0}^{\infty} 4\pi f^2 X^2_{mirror} df} \ . \qquad (3)$$

In practice, we use a simple trapezoidal rule to perform numerical integration from 0.1 to 10 Hz. The frequency axis is sampled densely to insure sufficient density of data to pick up the micro-seismic peak and stack resonances. Based on previous experience, it is believed[4] that RMS velocities of the order of 1 μm/sec should guarantee reasonable lock acquisition performance.

3.5 Calculation of Figures of Merit for Lock Maintenance

Whether the SUS actuators can maintain a lock condition depends on the amount of force required to control the mirrors and the force capacity of these actuators. A figure of merit χ_{RMS} is defined as the RMS value of a weighted mirror displacement measure $\chi(s)$ calculated as

$$\chi(s) = F^{-1}(s)\left(T^{SUS}_{xx}(s)\right)^{-1}\sqrt{X^2_{mirror}(s)}\,, \qquad (4)$$

where $F^{-1}(s)$ is the inverse of the SUS actuation compensation. The RMS value of $\chi(s)$ is computed by integration as

$$\chi_{RMS} = \sqrt{\int_{f=0}^{\infty} \chi(s)^2 df} \ . \qquad (5)$$

The SEI design requirement document[4] imposes an upper limit of 2.666 μm on χ_{RMS}.

As for the lock acquisition requirement, integral (5) is evaluated numerically using a trapezoidal rule. For typical stacks, the micro-seismic peak dominates χ_{RMS}, with small contributions from the first resonances of the stack. This implies that χ_{RMS} is only weakly dependent on the stack design (the Q's of the first few resonances for example).

4. Viton Spring Stack

4.1 Properties of Viton Springs

Description of these springs and calculation of their stiffnesses and loss factors are given in [7].

4.2 Stack Design

The design procedure outlined in [5] with 3 stages and a maximum load per spring equal to 556 N (125 lbs) leads to the stack design of Table 1. The total mass of 1765 kg (3893 lbs, includes stack, optics table, and payload) is adopted as an upper limit for the other two stacks in this document.

i (stage #)	M_i, kg (lb) (per leg)	# *springs / leg*	f_i (Hz)	P_i/P_{max} (%)
3 (top)	159 (351)	3	16.6	94
2	108 (239)	5	25.9	94
1 (base)	174 (383)	8	25.9	97

Number of legs	4
Total mass:	1765 kg
Total # springs:	64
$\log_{10}(T_{zz})$ @ 35Hz:	-1.17

Table 1: HAM stack design with VITON springs.

The table lists for each stage the mass per leg of the leg elements (or ¼ of the optics table weight for stage 4), the number of springs per leg, the uncoupled stage natural frequency f_i, and the load per spring expressed as a percentage of the assumed ultimate static load capacity.

In order to guarantee back and forth compatibility between the Viton and coil spring stacks (so as to maintain the Viton stack as a candidate last-minute fall-back position), and because the loaded Viton springs are substantially shorter than the loaded coil springs, we propose a Viton stack where the upper stage (3 springs per leg) is replaced with a two-layer stage of 3 springs on top of 3 more (see Fig. 4). The two layers are separated by a small circular plate. The mass of this plate is small enough that it does not behave as an additional stack stage (i.e. it does not introduce new dynamics at low frequency). The result is a top stage that behaves like it was made with springs 2 times softer than the original Viton spring, and a slight improvement in isolation performance.

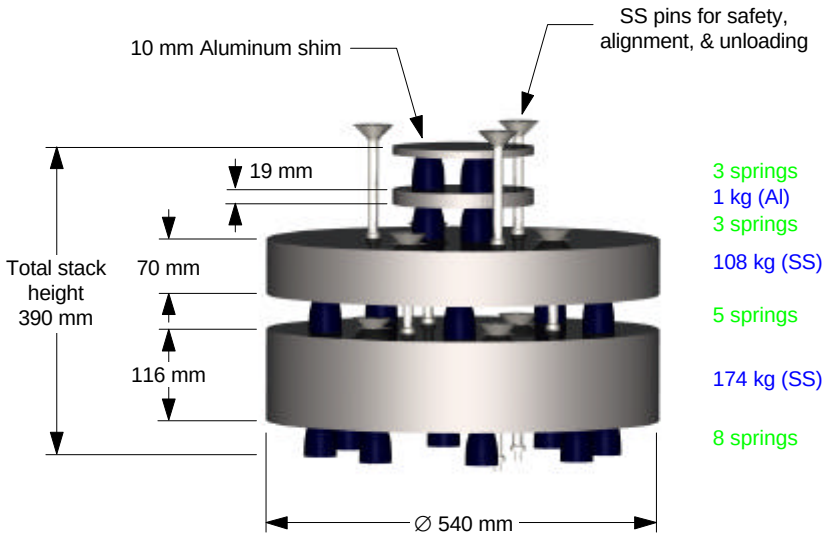

Figure 4: One leg of a VITON spring stack with double top stage.

The natural frequency of the longest safety pins (cantilevered) have been evaluated to about 180 Hz. Because at that frequency the actual horizontal isolation performance of the stacks is more than 4.5 orders of magnitude better than required, and because the pins only represent a small portion of the total stack mass, those resonances are not expected to create violations of the design requirements.

4.3 Performance Predictions

Nominal isolation performance in the horizontal and vertical directions is shown in Fig. 5. Note that, even with the the Viton springs, the isolation performance is much better than required.

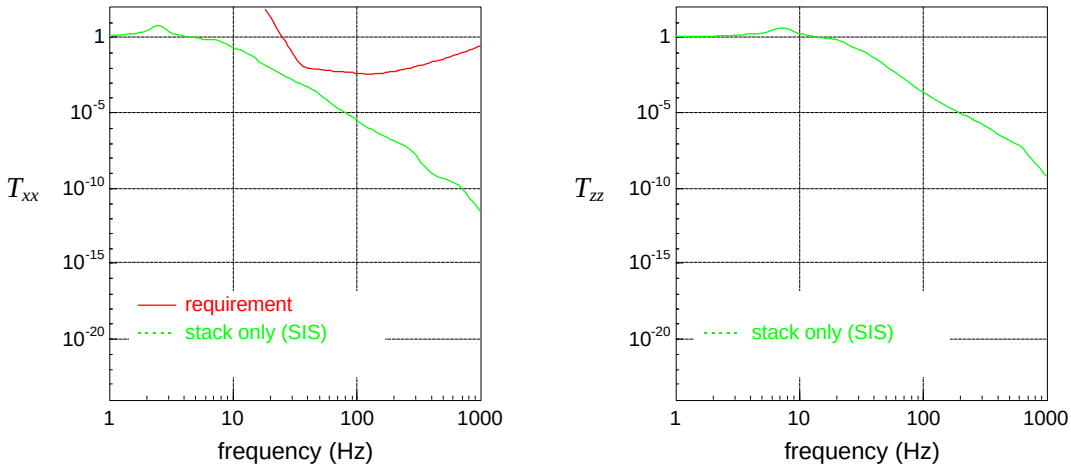

Figure 5: Nominal isolation performance of HAM stack with VITON springs compared to requirements.

Figure 6 shows the estimated residual mirror motion due to seismic noise. There is no explicit requirement on this spectrum. In addition to the total residual noise, the figure shows individual contributions from floor noise in X or Z direction alone. Note that at

frequencies below about 10 Hz, direct transmission of horizontal floor noise is the dominant contribution (the black curve is hidden behind the green in that range), while the conversion of vertical floor noise dominates at higher frequencies.

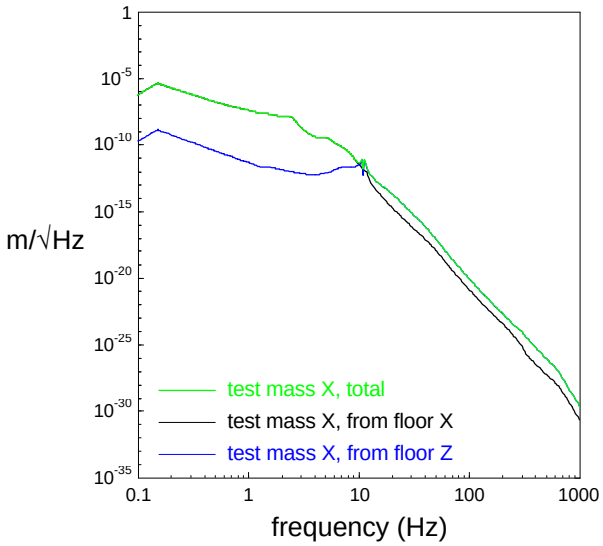

Figure 6: Spectrum of residual mirror motion for VITON springs stack; the green curve shows total residual seismic noise while the black and blue curves show contributions from horizontal and vertical floor noise, respectively.

Monte Carlo simulations were performed to evaluate the effect of stack imperfections as described in [8]. The results are very similar to those obtained for the BSC stacks, with very small variations in performance for imperfect stacks as compared to a perfect, nominal one. Those results are not included in this document.

The PSD of mirror *X* motion is then integrated (using very fine frequency resolution, however result is approximate) to evaluate the lock acquisition and maintenance criteria[4]. The values obtained are listed in Table 2 and compared to requirements.

	value	requirement
Lock Acquisition	1.21 μm/sec	~ 1 μm/sec
Lock Maintenance	2.10 μm	< 2.7 μm

Table 2: HAM stack with VITON springs. Lock acquisition and maintenance requirements.

5. Coil Spring Stack

5.1 Properties of Coil Spring

The coil spring is described in detail in [7]. Its geometry is shown in Fig. 7. The expected static axial load capacity is 445 N (100 lbs).

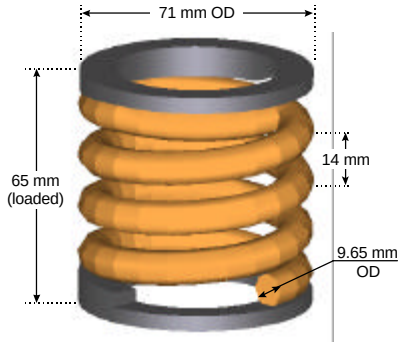

Figure 7: coil spring design.

Stiffnesses and loss factors in the axial direction are evaluated analytically as described in reference 7. The results presented here also use ratios of shear to axial stiffnesses and loss factors identified from single stage platform tests[9] and assumed frequency independent (k_{shear} / k_{axial} = 2.1 and h_{shear} / h_{axial} = 0.7).

5.2 Stack Design

The design procedure outlined in [5] with 3 stages and a maximum load per spring equal to 445 N (100 lbs) leads to the stack design of Table 3. Note that the total weight of this stack is identical to that of the baseline Viton stack of Table 2.

i (stage #)	M_i, kg (lb) (per leg)	# *springs / leg*	f_i (Hz)	P_i/P_{max} (%)
3 (top)	159 (351)	4	6.5	88
2	108 (239)	6	9.8	97
1 (base)	174 (383)	10	9.8	97

Number of legs	4
Total mass:	1765 kg
Total # springs:	80
$\log_{10}(T_{zz})$ @ 35Hz:	-3.68

Table 3: HAM stack design with COIL springs.

The stack is shown in Fig. 8. As mentioned in section 4.2, the leg elements and total stack height are the same as those of the Viton stack.

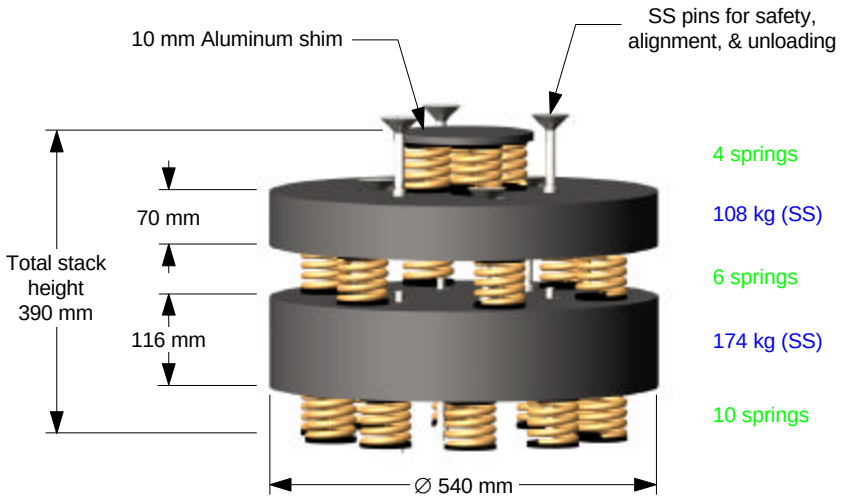

Figure 8: One leg of a COIL spring stack.

5.3 Performance Predictions

Predicted performance of the nominal stack is shown in Fig. 9. Note again that the requirements are satisfied with a large margin.

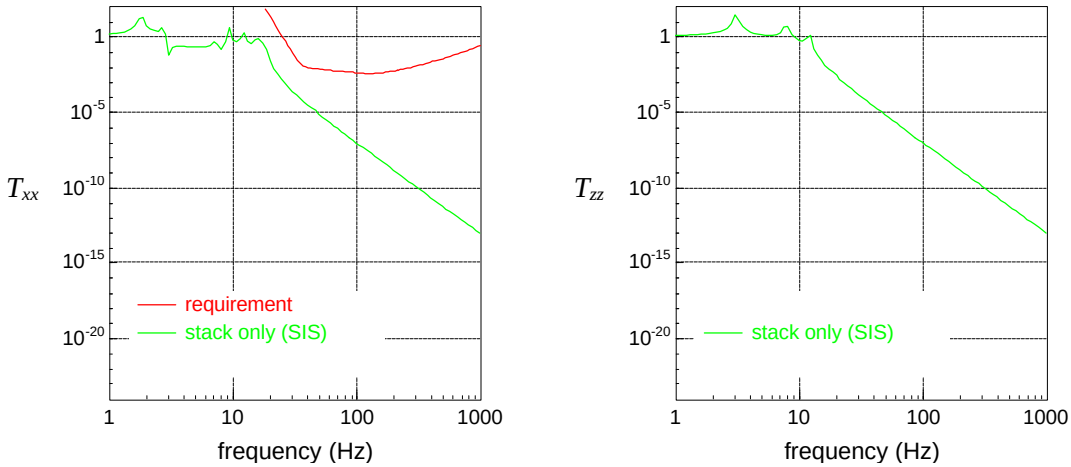

Figure 9: Nominal isolation performance of HAM stack with COIL springs compared to requirements.

Predicted spectrum of mirror *X* motion is shown in Fig. 10. Note that, in contrast with the Viton stack of Figure 6, direct transmission of horizontal floor noise dominates the total residual mirror noise at all frequencies.

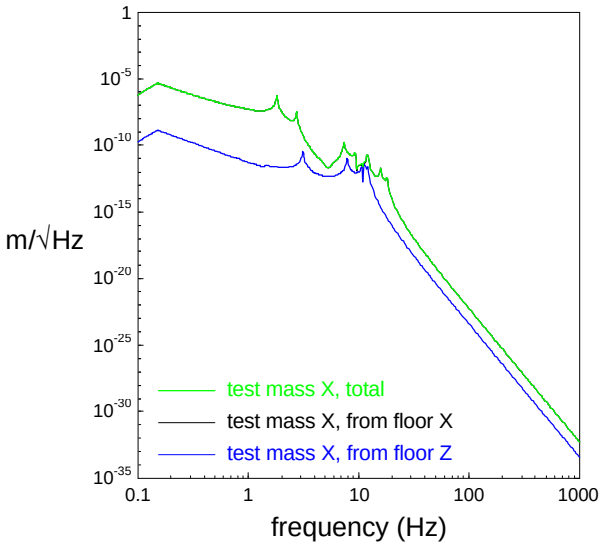

Figure 10: Spectrum of residual test mirror motion for COIL springs stack;

Monte Carlo simulations for imperfect stacks have shown the sensitivity to imperfections to be small. These results are not included here.

The values obtained for the lock acquisition and maintenance criteria are listed in Table 4 and compared to requirements.

	value	requirement
Lock Acquisition	1.94 μm/sec	~ 1 μm/sec
Lock Maintenance	2.51 μm	< 2.7 μm

Table 4: HAM stack with COIL springs. Lock acquisition and maintenance requirements.

6. Leaf Spring Stack

6.1 Properties of Leaf Spring

These springs (Fig. 11) are described in detail in [7]. Their expected static axial load capacity is 556 N (125 lbs).

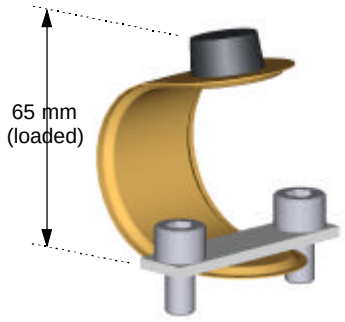

Figure 11: leaf spring geometry.

Dynamic properties (stiffness and damping VS frequency) were obtained from FEM analysis as described in [7]. The detailed design of the interfaces with the leg elements is not completely defined at this time; it is expected however, that the height under load of those springs will be the same as that of the coil springs, providing again a direct back and forth compatibility with the other two stacks.

6.2 Stack Design

The stack design procedure[5] with 3 stages and a maximum load per spring equal to 556 N (125 lbs) leads to the stack design of Table 5. Note again that the total weight of this stack is identical to that of the baseline Viton stack of Table 2.

i (stage #)	M_i, kg (lb) (per leg)	# *springs / leg*	f_i (Hz)	P_i/P_{max} (%)
3 (top)	159 (351)	3	6.5	94
2	108 (239)	5	10.2	94
1 (base)	174 (383)	8	10.2	97
		Number of legs	4	
		Total mass:	1765 kg	
		Total # springs:	64	
		$\log_{10}(T_{zz})$ @ 35Hz:	-3.60	

Table 5: HAM stack design with LEAF springs.

Again, this stack uses the same leg elements as both the Viton spring stack and the Coil spring stack and occupies the same vertical space (Fig. 12).

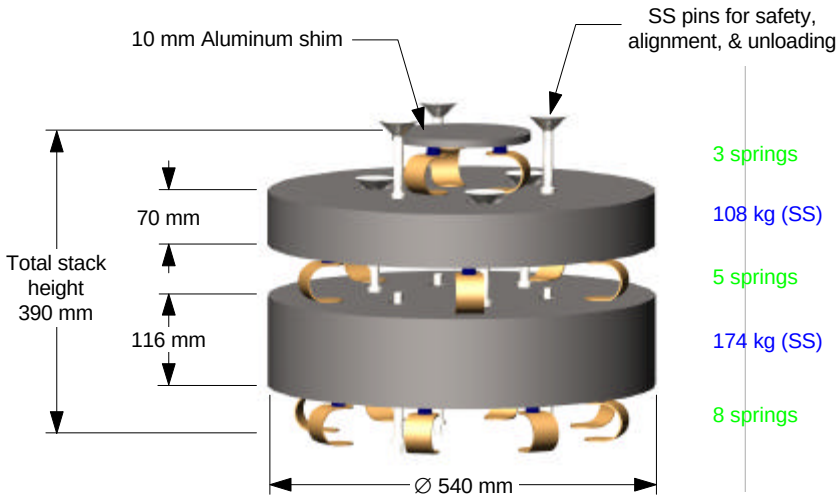

Figure 12: One leg of a LEAF spring stack.

6.3 Performance Predictions

The predicted performance of the nominal stack is shown in Fig. 13. Again, the requirement is clearly satisfied and the margin should be wide enough to absorb resonances of the support assembly.

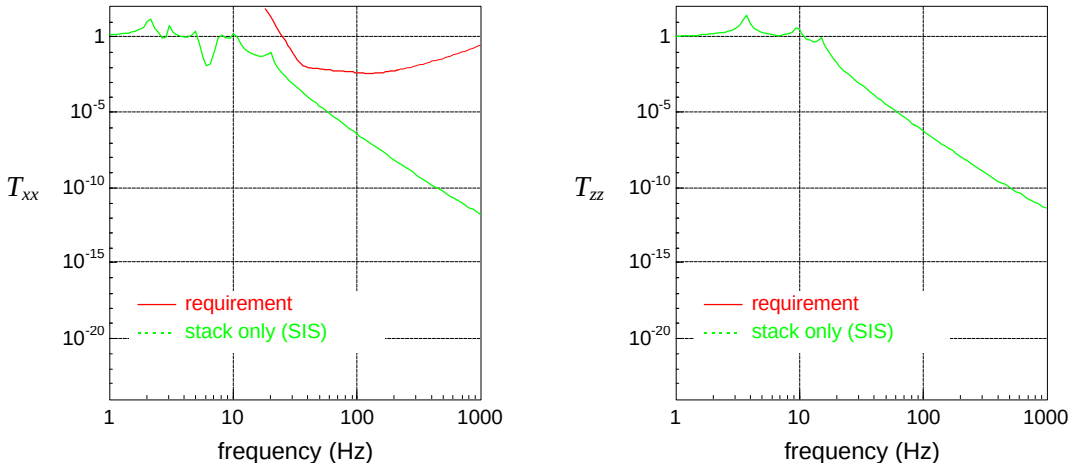

Figure 13: Nominal isolation performance of HAM stack with LEAF springs compared to requirements.

The spectrum of mirror motion in the *X* direction is shown in Fig. 14. Like in the case of the coil spring stack, direct transmission of horizontal floor noise dominates at all frequencies.

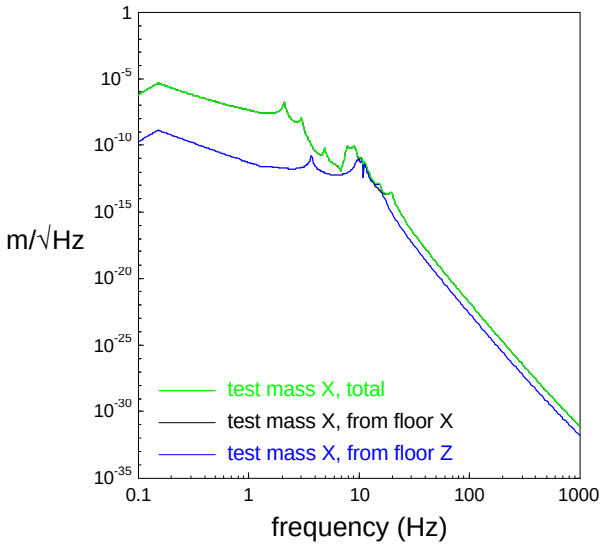

Figure 14: Spectrum of residual mirror motion for LEAF springs stack.

The values obtained for the lock acquisition and maintenance criteria are listed in Table 6 and compared to requirements.

	value	requirement
Lock Acquisition	1.42 μm/sec	~ 1 μm/sec
Lock Maintenance	2.29 μm	< 2.7 μm

Table 6: HAM stack with LEAF springs. Lock acquisition and maintenance requirements.

7. References

1. B. Weinstein, *HAM Support Assembly - Analytical Design*, HYTEC Inc., Los Alamos, NM, document HYTEC-TN-LIGO-12, January 1997.
2. E. Ponslet, *Isolation Stacks Preliminary Design Methodology*, HYTEC Inc., Los Alamos, NM, document HYTEC-TN-LIGO-02, February 21, 1996.
3. E. Ponslet and B. Weinstein, *HAM Optics Table - Mechanical Design and Analysis*, HYTEC Inc., Los Alamos, NM, document HYTEC-TN-LIGO-11, January 1997.
4. F. Raab and N. Solomonson, *Seismic Isolation Design Requirements Document* (draft and early corrections), LIGO draft document LIGO-T960065-02-D, California Institute of Technology and Massachusetts Institute of Technology, April 15, 1996.
5. E. Ponslet, *BSC Stack Design Trend Study*, HYTEC Inc., Los Alamos, NM, document HYTEC-TN-LIGO-03, March 1st, 1996.
6. S. Kawamura, *Response of Pendulum to Motion of Suspension Point*, LIGO document LIGO-T960040-00-D, California Institute of Technology and Massachusetts Institute of Technology, March 11, 1996.

7. E. Ponslet, *Design of Vacuum Compatible Damped Metal Springs for Passive Isolation of The LIGO Detectors*, HYTEC Inc., Los Alamos, NM, document HYTEC-TN-LIGO-04a (revision *a*), January 1997.
8. E. Ponslet, *BSC Seismic Isolation - Projected Performance Update*, HYTEC Inc., Los Alamos, NM, document HYTEC-TN-LIGO-07a (revision *a*), January 1997.
9. E. Ponslet, *LIGO Coil Springs - Test Report*, HYTEC Inc., Los Alamos, NM, document HYTEC-TN-LIGO-14, February 1997.
10. S. Kawamura, *Response of Suspension System to Pitch Motion of Suspension Point*, LIGO document LIGO-T960158-00-D, California Institute of Technology and Massachusetts Institute of Technology, September 26, 1996.

Note 1, Linda Turner, 09/03/99 11:40:15 AM
LIGO-T970238-00-D